Energy Storage Materials 41 (2021) 554–562

Contents lists available at ScienceDirect

Energy Storage Materials

journal homepage: www.elsevier.com/locate/ensm

2D titanium and vanadium carbide MXene heterostructures for electrochemical energy storage

Armin VahidMohammadi [a,1], Wentao Liang [b], Mehrnaz Mojtabavi [c], Meni Wanunu [c,d], Majid Beidaghi [a,*]

[a] Department of Mechanical and Materials Engineering, Auburn University, Auburn, AL 36849, United States
[b] Kostas Advanced Nanocharacterization Facility (KANCF), Northeastern University, Burlington, Massachusetts 01803, United States
[c] Department of Bioengineering, Northeastern University, Boston, Massachusetts 02115, United States
[d] Department of Physics, Northeastern University, Boston, Massachusetts 02115, United States

ARTICLE INFO

Keywords:
MXene
Heterostructure
Supercapacitor
Titanium carbide
Vanadium carbide

ABSTRACT

Two-dimensional (2D) heterostructured electrodes built from vertical stacking of different 2D materials are among the most promising electrode architectures for electrochemical energy storage devices. These materials offer interesting opportunities for energy storage applications such as versatility in the structural design of electrode, and the possibility to integrate individual 2D building blocks with different properties into heterostructures. These features can potentially enable new materials with improved or new electrochemical features. Here, we report on large-scale liquid phase self-assembly of 2D heterostructures built from two different 2D transition metal carbides (MXenes), $Ti_3C_2T_x$ and V_2CT_x. A cation-driven self-assembly process was used to assemble the negatively-charged flakes of the two MXenes into heterolayered flakes. The freestanding and binder-free MXene heterostructure films could deliver a high volumetric capacitance of ~1473 F cm^{-3} and showed no capacitance loss after 50,000 charge-discharge cycles in 3 M H_2SO_4 electrolyte. Due to coupling of redox reactions of $Ti_3C_2T_x$ and V_2CT_x, the heterostructure electrodes showed a nearly constant current over their entire potential window, which is reminiscent of traditional pseudocapacitive materials. This electrochemical behavior differs from individual MXene electrodes or most other emerging pseudocapacitive materials whose maximum performance is usually achieved in a narrow potential range.

1. Introduction

Two-dimensional (2D) materials offer interesting properties such as high surface areas, accessible redox-active sites, exceptional ion and charge transport properties, and excellent mechanical robustness, all of which make these materials promising for electrochemical energy storage applications [1]. However, these properties are largely dependent on the specific type and composition of 2D materials, and only a few 2D material may offer all of these properties combined [1–3]. Additionally, inherent properties, such as low electrical conductivity and highly exposed surfaces of many 2D materials used for energy storage applications, can result in slow charge transfer properties or unwanted side reactions with electrolyte and other cell components, resulting in their poor cyclic stability (i.e., many 2D metal oxides suffer from these issues) [1]. Sequential stacking of different 2D materials to produce heterostructures is considered as an effective approach to synthesize materials with superior physical and (electro)chemical properties [1,2,4–6]. Such 2D heterostructures can not only potentially eliminate major shortcomings of individual 2D materials, but also enable the realization of numerous new electrode compositions with diverse properties for batteries and supercapacitors [1].

2D transition metal carbides and nitrides, MXenes, have received considerable attention in a wide range of applications from electromagnetic interference shielding to biomolecule sensing [7–12]., and in particular, as promising electrode materials for energy storage devices because of their high electrical conductivities, cation intercalation capability, and high-rate pseudocapacitive properties [13–17]. MXenes distinguish themselves from other 2D materials by their diverse compositions and structures. With a general formula of $M_{n+1}X_nT_x$ (M is a transition metal, X is carbon/nitrogen, n can be 1 to 4, and T_x represents different surface functional groups) [14,18], to date, more than 30 different MXenes are experimentally synthesized and many more have been theoretically predicted [13,19]. Therefore, this large family of 2D materials provide an excellent model system to explore the properties of 2D heterostructures and heterolayered electrodes.

* Corresponding author.
E-mail address: mbeidaghi@auburn.edu (M. Beidaghi).
[1] Current address: A. J. Drexel Nanomaterials Institute, Department of Materials Science and Engineering, Drexel University, Philadelphia, PA 19104, USA.

https://doi.org/10.1016/j.ensm.2021.06.014
Received 1 April 2021; Received in revised form 30 May 2021; Accepted 10 June 2021
Available online 12 June 2021

Recently, a few examples of heterostructures of $Ti_3C_2T_x$ MXene with other 2D materials have been reported [20–26]. While these early studies have suggested enhanced properties for the final hetero (or hybrid) materials, the stacking order in these 2D assemblies is often random. In addition, these early reports have only focused on the combination of 2D $Ti_3C_2T_x$ with graphene or 2D transition metal oxides and dichalcogenides, leaving behind other promising pseudocapacitive MXene compositions such as Ti_2CT_x and V_2CT_x, as well as the possibility of synthesizing all-MXene heterostructures by stacking of different MXene compositions. In most cases, this is due to the lack of established methods for the controlled synthesis and delamination of other MXenes and the low chemical stability of some MXene compositions. Recently, we reported on highly stable 2D vanadium carbide (V_2CT_x) pillared films and their exceptional performance as supercapacitor electrode materials [16]. The outstanding performance of 2D V_2CT_x showed that the pseudocapacitive performance of MXene is not limited to $Ti_3C_2T_x$. In fact, a recent computational study has predicted superior pseudocapacitive properties for many other MXenes [27]. Nevertheless, these MXenes still need to be assembled into structures with high ionic and electronic transport properties to be used as electrode materials for pseudocapacitive energy storage. We argue that controlled stacking of different 2D MXene sheets might enable the realization of heterostructure MXene materials that address shortcomings of individual MXenes and result in superior chemical, electrochemical, and physical properties.

Here we report on the large-scale self-assembly of 2D heterostructures from liquid dispersions of two different MXenes, namely, three atomic-layer-thick V_2CT_x and five atomic-layer-thick $Ti_3C_2T_x$ as model compositions. The assembled structures display a high order in their stacking sequence. The freestanding binder-free films fabricated from assembled MXene heterolayers show new electrochemical features and improved performances with a high volumetric capacitance of ~1473 F cm^{-3} and exceptional cycle life with a ~8% capacitance increase after 50,000 cycles in 3 M H_2SO_4 electrolyte. These metrics surpass the performances of both individual $Ti_3C_2T_x$ and V_2CT_x MXene electrodes.

2. Experimental section

2.1. Synthesis and delamination of MXenes

$Ti_3C_2T_x$ and V_2CT_x MXenes were synthesized by selective etching of their respective MAX phases, Ti_3AlC_2 and V_2AlC in acidic solutions [12,47–49]. Ti_3AlC_2 was prepared by mixing TiC (99.5%, ~ 2 μm, Alfa Aesar, Al (99.5%, 325 mesh, Alfa Aesar), and C powders (99%, 325 mesh, Alfa Aesar) in a 2:1:1 ratio. The powders were ball milled using zirconia balls for 18 h and then sintered at 1400 °C for 2 h under flowing argon atmosphere. V_2AlC MAX phase was synthesized according to previous reports [16,48]. To synthesize delaminated $Ti_3C_2T_x$ (*d*-$Ti_3C_2T_x$) MXene, typically 2 g of Ti_3AlC_2 powder was slowly added to a mild etchant consisting of 2 g LiF (98.5%, Alfa Aesar) in 40 mL 6 M HCl (ACS grade, BDH) [49,50]. The etching reaction was carried out for 24 h at 35 °C and then the etched powders were washed several times until the pH of the solution was ~ 6. Then the powders were collected and redispersed in 150 mL DI water and probe sonicated for 1 h. The final *d*-$Ti_3C_2T_x$ solution was obtained by centrifuging the dark sonicated solution for 1 h at 3500 rpm and collecting the supernatant. Delaminated V_2CT_x (*d*-V_2CT_x) solutions were prepared according to our previous work [16]. Since *d*-V_2CT_x is very unstable in aqueous solution, the processing and fabrication of heterostructures were performed immediately after *d*-V_2CT_x dispersions were obtained.

2.2. Assembly of MXene heterostructures from the liquid phase

To assemble heterolayered MXenes and their corresponding heterostructure films, *d*-$Ti_3C_2T_x$ and *d*-V_2CT_x solutions were mixed in different ratios. This resulted in stable mixture solutions since both MXene have similar negative zeta potentials in water [9,29]. Then a solution of saturated NaCl (based on our previous work [16], this can be done with other alkali solutions as well) was added to the mixture solution while being stirred slowly. This resulted in rapid self-assembly of MXenes and their precipitation at the bottom of the container. The supernatant was poured out, and the precipitates were washed several times to remove the excess salt. In order to fabricate the freestanding films, dispersions of heterolayered flakes were gently shaken to obtain a uniform dispersion and then vacuum filtered on top of a piece of Celgard membrane. The fabricated MXene heterostructure films were labeled as Na-(Wt.% of $Ti_3C_2T_x$-Wt.% of V_2CT_x). For example, a heterostructure film with a $Ti_3C_2T_x$ to V_2CT_x weight ratio of 60:40 was labelled as Na-(60–40). Through this simple and rapid assembly, up to 0.5 g of heterolayered MXene flakes could be produced in one batch.

2.3. Characterization techniques

XRD analyses were carried out at a scan speed of 0.2 s per 2θ step using Bruker X-ray diffractometer (D8 Discover) with 40 kV and 40 mA Cu-kα radiation. SEM/EDS analyses of the samples were done using a JEOL JSM-7000F scanning electron microscope. To prepare samples for S/TEM analyses, initially, a FEI Scios dual beam system with gallium ion beam source was used to prepare lamellae from a cross-section of 2D MXene heterostructure films. Then, lamellas were thinned to a thickness of less than 100 nm and placed on a TEM grid. Imaging of lamellas was performed with a probe-corrected FEI Titan Thermis 300 S/TEM with ChemisSTEM technology in both HR-TEM and STEM imaging modes. TEM based EDS mapping was performed at 300 kV using a SuperX EDS system.

2.4. Electrochemical measurements

Plastic Swagelok cells were used in all the electrochemical measurements. Glassy carbon electrodes were used as current collectors for both the working and counter electrodes. In all three-electrode experiments, Ag/AgCl wire immersed in 3.5 M KCl was the reference electrode. Working electrodes (WE) were prepared by directly punching the freestanding MXene heterostructure films. An over-capacitive activated carbon film (YP-50), prepared according to previous reports [15,16], was used as the counter electrode (CE) in the cells. A 3 M H_2SO_4 solution was used as the electrolyte in all cells. After their assembly and before electrochemical measurements, cells were rested for 1 h and then cycled for at least 50 times at a scan rate of 20 mV s^{-1} to stabilize their performance. Cyclic Voltammetry (CV) experiments were carried out at scan rates ranging from 2 mV s^{-1} to 10 Vs^{-1}. Cycle life of the electrodes was examined by galvanostatic charge/discharge experiments at a current density of 10 A g^{-1} for 10 000 cycles. Electrochemical impedance spectroscopy (EIS) data were collected in the 100 mHz to 1000 kHz frequency range. The applied potential amplitude was 10 mV. Symmetric supercapacitors (full cells) were assembled by using two similar MXene heterostructure electrodes (similar weights and thickness) as working and counter electrodes. The specific capacitance of the full cells was calculated considering the total weight (or volume) of both electrodes.

The capacitance of the electrodes was calculated from the reduction portion of the CV profiles at different scan rates by using the following equation:[28]

$$C = \frac{1}{\Delta V}\int \frac{j\,dV}{s} \tag{1}$$

where C is the normalized capacitance (F cm^{-3} or F g^{-1}), ΔV is the voltage window (V), j is the current density (mA cm^{-3} or mA g^{-1}), V is voltage (V), and s is the scan rate (mV s^{-1}). Also, the specific energy (E) and power (P) densities of the symmetric cells were calculated from CV graphs at different scan rates using the following equations: [15]

$$E = \left(\frac{1}{2}\times C\times V^2\right)/3600\left[\mathrm{Whcm^{-3}}\right] \tag{2}$$

$$P = E\times\frac{s}{V}\times\ 3600\left[\mathrm{Wcm^{-3}}\right] \tag{3}$$

where C is the normalized capacitance of the device (F cm^{-3}), V is the operating potential window (V), and s is the scan rate (V s^{-1}).

The contributions of different charge storage mechanisms in the electrodes were explained by considering a power-law relationship between the current, i, and scan rate, v ($i = av^b$). $b = 0.5$ indicates a diffusion-controlled process and $b = \sim 1$ corresponds to a surface-controlled charge storage mechanism [45]. Contribution of each mechanism in the total stored charge was calculated through considering a combination of capacitive controlled and diffusion controlled mechanisms at the corresponding current value of each potential point, according to the following equation: [28]

$$i(V) = k_1 v + k_2 v^{0.5} \quad (4)$$

In the above equation, V is the potential and k_1 and k_2 are variables. $k_1 v$ indicates a capacitive contribution and $k_2 v^{0.5}$ determines the diffusion-controlled contribution.

3. Results and discussion

The $Ti_3C_2T_x$-V_2CT_x MXene heterostructures were prepared by charge-induced self-assembly [16,26] of negatively charged [9,28,29] MXenes' mixture dispersions and through addition of saturated alkali salt solutions. This approach is different than the method widely used in the liquid-phase assembly of 2D heterostructures which rely on the electrostatic self-assembly of two oppositely charged 2D materials [6,25,30,31]. Despite the promise of the electrostatic self-assembly approach, it is not applicable to assemble different MXenes into heterostructures since the selective etching process used in the synthesis of MXenes results in their functionalized surfaces that are negatively charged in water dispersions [14]. Therefore, because of their similarly charged surfaces, the colloidal mixture of various MXenes is also stable. In addition, although having two oppositely charged 2D materials seems to be favorable for assembly of unilamellar 2D heterostructures [32,33], the large organic polycations (i.e., polydiallyldimethylammonium chloride, PDDA or aminosilane coupling agent in case of MXene [34]) that are usually used to prepare the positively charged 2D materials, result in large insulating gaps (and not an intimate contact) between assembled flakes, decreasing the electrical conductivity of the fabricated electrodes [25]. Also, using large organic polycations limits the precise assembly of ordered multilayers with single-layer precision [35]. In contrary, as we have recently demonstrated [35], using small molecules with high charge densities can enable fabrication of pillared multilayer structures with precise stacking. In the present work, negatively charged $Ti_3C_2T_x$ and V_2CT_x flakes were assembled into heterolayered structures using Na^+ cations to induce self-assembly. Fig. 1**a** schematically shows the assembly process. In short, aqueous dispersions of $Ti_3C_2T_x$ and V_2CT_x MXenes were separately prepared and mixed in different weight ratios. Then, saturated solution of sodium chloride was added to these colloidal mixtures to self-assemble the MXene flakes [16] (see details in the Experimental Section). We chose to perform the assembly process using Na^+ because in our previous work on the assembly of V_2CT_x, the multilayered flakes assembled with Na^+ showed the best electrochemical performance [16]. However, in principal the assembly process can be performed using other cations [16,36,37]. For comparison, the same assembly process was used to prepare multilayered flakes of $Ti_3C_2T_x$ and V_2CT_x. The assembled multilayered or heterolayered flakes were redispersed in water and used in the fabrication of freestanding films by vacuum assisted filtration. Fig. 1**b** shows digital photographs of the freestanding films fabricated using assembled multilayered MXenes (a.k.a. Na-$Ti_3C_2T_x$ and Na-V_2CT_x) and the heterostructure $Ti_3C_2T_x$-V_2CT_x film with a weight ratio of 60:40 (referred to as Na-(60–40)). The $Ti_3C_2T_x$ film has a dark gray color, and V_2CT_x film shows a light gold brownish color, while the Na-(60–40) MXene heterostructure film shows a uniform and dark grayish brown color. No visual color variation/separation along the film could be seen, suggesting uniform assembly of 2D layers without apparent agglomeration of individual MXenes in the macroscale. A cross-sectional scanning electron microscopy (SEM) image of the heterostructure film (shown in Fig. 1**c**) showed layered stacking of 2D nanosheets that are typical of vacuum filtered films.

X-ray diffraction (XRD) analyses was carried out to understand the structure and stacking order of the fabricated all-MXene heterostructure films at different weight ratios. Fig. 2**a** shows the XRD patterns of the pristine MXene films fabricated by vacuum filtration of the delaminated V_2CT_x (*d*-V_2CT_x) and d-$Ti_3C_2T_x$ MXene solutions, as well as films fabricated using Na-$Ti_3C_2T_x$ and Na-V_2CT_x multilayer flakes. Due to the intercalation of large TBA^+ cations in the delamination process, the d-V_2CT_x shows a very large interlayer spacing of 15.41 Å. In agreement with our previous results [16], assembly of d-V_2CT_x with Na^+ cations resulted in a large upshift in the position of the peak corresponding to (0002) basal planes of V_2CT_x (from 5.73° to 8.47°, $\delta_{d(0002)}$ = 4.98 Å), suggesting the exchange of larger TBA^+ ions with smaller high charge density Na^+ ions where the sodium cations pull the negatively charged MXene sheets together. In contrast, the Na-$Ti_3C_2T_x$ film showed a slightly larger d-spacing of 12.7 Å (compared to 12.49 Å for d-$Ti_3C_2T_x$), probably, as the result of the (partial) substitution of Li cations remained from etching and delamination process of $Ti_3C_2T_x$ with larger Na^+ cations [38].

Fig. 2**b** shows the evolution of the (0002) basal plane peaks of heterostructure MXene films assembled using various $Ti_3C_2T_x$ to V_2CT_x ratios. These ratios were selected using a previously proposed method based on a hypothetical surface area-matching model for 2D materials [30,33] to calculate an initial composition for mixing $Ti_3C_2T_x$ and V_2CT_x flakes (see SI for calculations). Accordingly, to match their surface areas in the dispersion the required weight ratios of $Ti_3C_2T_x$ to V_2CT_x was calculated to be ~1.5 (60:40). Then, other assemblies with other compositions were prepared by changing the V_2CT_x:$Ti_3C_2T_x$ weight ratio. The XRD spectra of heterostructure films showed a pair of peaks corresponding to (0002) basal planes of the Na-$Ti_3C_2T_x$ and Na-V_2CT_x with very marginal shifts from their original position ($\delta_{d(0002)}$ = +0.4 Å and −0.4 Å, respectively). The intensity of the (0002) peak corresponding to Na-V_2CT_x increased gradually by increasing the weight ratio of V_2CT_x in the assembled heterostructure films while the intensity of the (0002) basal plane peak for Na-$Ti_3C_2T_x$ decreased. These observations suggest a change in the stacking number of individual MXene sheets in the fabricated heterolayered films, similar to the one-dimensional two-phase model proposed by Onada et al. [39] with no phase-separation (suggested structures are schematically shown in **Fig. S1**). To further support our hypothesis, we performed XRD analysis on the heterolayered flakes in their powder forms (the precipitated powders after assembly and not the films prepared by vacuum filtration) which showed only a single peak in the low angle region and lacked the individual peaks corresponding to Na-$Ti_3C_2T_x$ or Na-V_2CT_x (**Fig. S2**). These results suggest that our observation of two separate peaks in the heterostructure films is not due to phase separation and is related to the directional ordering of the assembled heterolayered flakes in the vacuum filtered films. Importantly, co-existence of the (0002) basal plane peaks was not observed in a control sample prepared by only mixing the two MXene solutions and vacuum filtration (**Fig. S3**). This can be attributed to a completely random mixture of the two MXene compositions, which further signifies the role of cations in the assembly process [39,40]. The decreased intensity and broad nature of the (0002) peaks for the 2D MXene heterostructure films, however, indicate imperfections in the stacking number and sequence of the $Ti_3C_2T_x$ and V_2CT_x MXene sheets, and potentially misorientation of (0002) planes with respect to each other [6,30].

Atomic force microscopy (AFM) images and the corresponding height profiles of the single-layer $Ti_3C_2T_x$, V_2CT_x, and their Na-(60–40) heterolayer flakes are shown in Fig. 2**c-e** (also **Fig. S4**), respectively. The larger measured thicknesses of single-layer flakes compared to their theoretical values are in agreement with previous reports and originate from trapped water molecules and intermolecular interactions between

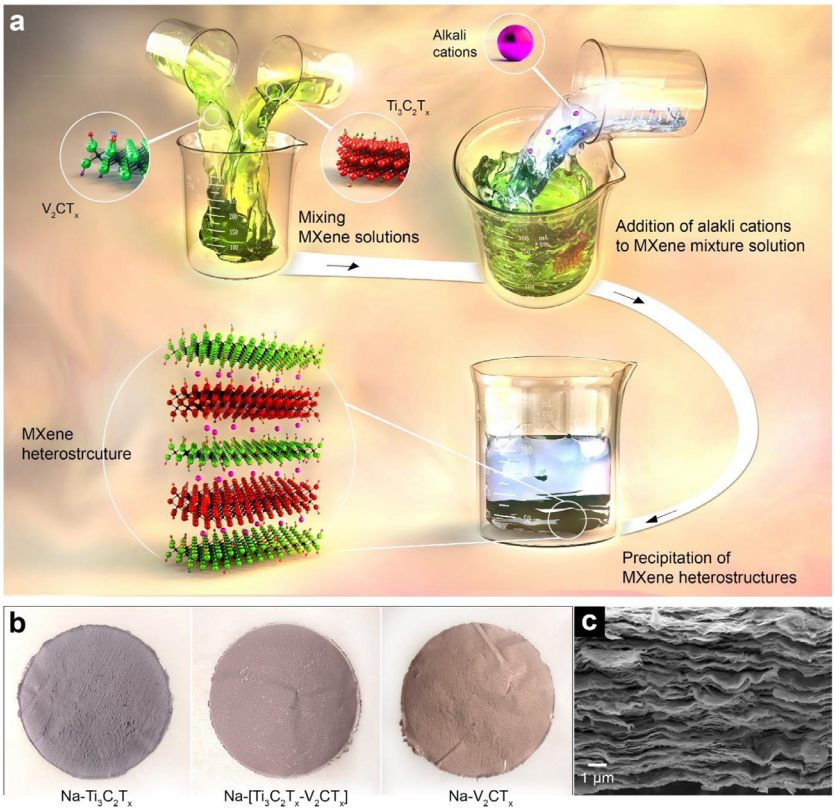

Fig. 1. Self-assembly process for MXene heterostructures. (a) Schematic illustration depicting the cation-induced self-assembly of MXenes. (b) Digital photographs of the free-standing binder-free films of $Ti_3C_2T_x$, MXene heterostructure ($Ti_3C_2T_x$:V_2CT_x of 60:40), and V_2CT_x assembled with Na cations. These films were prepared by vacuum-assisted filtration. (c) A cross-sectional SEM image of a Na-(60–40) MXene heterostructure film, demonstrating its layered structure.

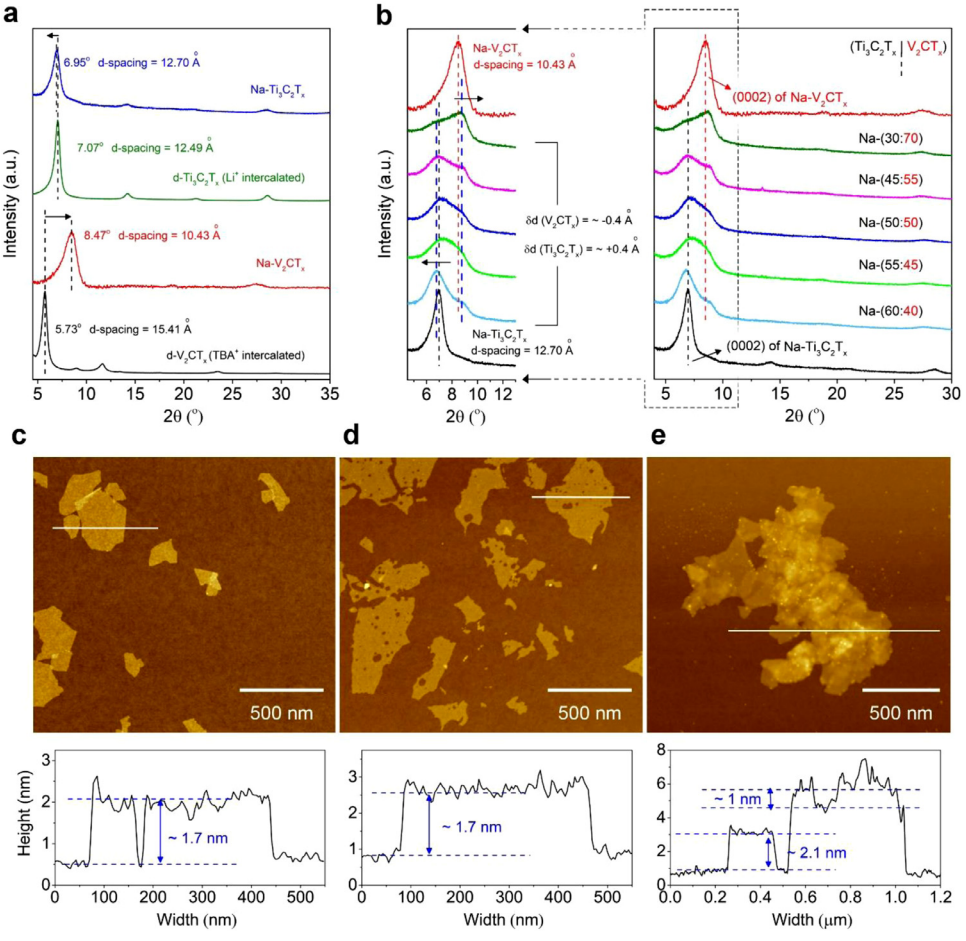

Fig. 2. Structural characterization of the MXene heterostructure films. (a) XRD patterns of $Ti_3C_2T_x$ and V_2CT_x, and their Na-assembled films, showing the change in $d_{(0002)}$ upon self-assembly for different MXenes. (b) XRD patterns of the different MXene heterostructure films showing the change in the intensity and position of the (0002) peak for $Ti_3C_2T_x$ and V_2CT_x MXenes by changing the composition of films. The left graph in panel b shows enlarged portion of the right XRD patterns between 7 and 12°. AFM images and the corresponding height profiles of the (c) $Ti_3C_2T_x$, (d) V_2CT_x, and (e) heterolayered MXene flakes assembled with Na cations with a $Ti_3C_2T_x$ to V_2CT_x ratio of 60:40.

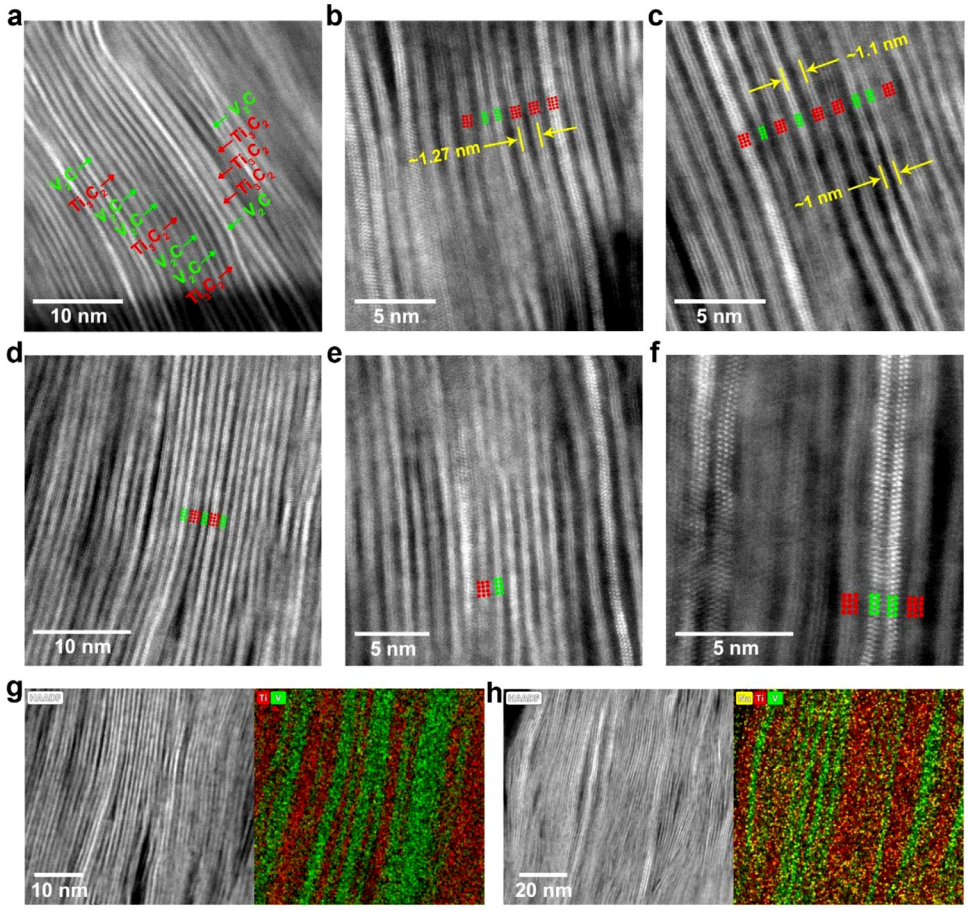

Fig. 3. Transmission electron microscopy (TEM) analysis of the MXene heterostructure films. (a) A high-resolution TEM image of Na-assembled MXene heterostructure films with a $Ti_3C_2T_x$ to V_2CT_x weight ratio of 60:40, referred to as Na-(60–40), showing the alternating sequence of the two MXene compositions along the cross-section of the film. (b, c) STEM atomic-resolution images of the Na-(60–40) films and the measured average spacings between individual $Ti_3C_2T_x$ and V_2CT_x stackings as well as the spacing between face-to-face $Ti_3C_2T_x$ and V_2CT_x sheets. (d) High-resolution TEM and (e-f) STEM atomic-resolution images of a Na-(45–55) MXene heterostructure film, showing the difference in the sequencing and the stacking number of the $Ti_3C_2T_x$ and V_2CT_x MXene sheets compared to the Na-(60–40) composition. High-angle annular dark-field (HAADF) TEM images and EDS maps of the (g) Na-(60–40) and (h) Na-(45–55) heterostructure films.

MXenes' surface groups and the silicon substrate [9,41]. Nevertheless, stacking of MXene nanosheets and the significantly higher thickness of the heterolayered MXene flakes is evident in Fig. 2**e**. High-resolution and scanning transmission electron microscopy (HR-TEM / STEM) was used for a more detailed study of the stacking sequence and the structure of the fabricated heterolayers. Since V_2CT_x is three-atomic-layer thick but $Ti_3C_2T_x$ is five-atomic-layer thick, these two MXenes are easily distinguishable in HR/S-TEM images.

A HR-TEM image and scanning transmission electron microscopy (STEM) images of a sample prepared from a Na-(60–40) heterostructure film are shown in Fig. 3**a-c**. These images demonstrate face-to-face sequential stacking of $Ti_3C_2T_x$ and V_2CT_x sheets in the heterostructure films. TEM images showed larger stacks of $Ti_3C_2T_x$ compared to V_2CT_x stacks, in good agreement with the XRD results of Na-(60–40) sample where the peak corresponding to $Ti_3C_2T_x$ has a higher intensity (Fig. 2**b**). The average interlayer spacings for stacks of $Ti_3C_2T_x$ (~1.27 nm) and V_2CT_x (~1 nm) measured from STEM images are in good agreement with the values calculated from the XRD analyses. Furthermore, from the STEM images, the average inter-flake distance between the neighboring $Ti_3C_2T_x$ and V_2CT_x layers was measured to be ~ 1.1 nm. A similar value (~ 1.15 nm) can be roughly calculated from the XRD results considering the center of the broad (0002) peaks of the heterostructure films as the average representing distance for the assembled flakes (assuming perfect stacking where the two peaks merge into one broad peak). Fig. 3**d** shows the HR-TEM image of a Na-(45–55) heterostructure film, and Fig. 3**e, f** show the corresponding STEM images. For this composition, similar flake stacking can be seen while, and in agreement with the XRD results, here the number of V_2CT_x stacks are larger than the $Ti_3C_2T_x$ stacks. Fig. 3**g, h** show TEM/EDS elemental maps of a Na-(45–55) heterostructure film, confirming successive assembly of few-layer stacks of $Ti_3C_2T_x$ and V_2CT_x. Fig. 3**h** also shows the presence of Na atoms. It is noteworthy that TEM images of $Ti_3C_2T_x$ and V_2CT_x (60–40) mixture films (fabricated without self-assembly process, shown in **Fig. S5**) showed a random stacking of the two MXenes with no obvious pattern, in good agreement with the XRD results shown in **Fig. S3**.

Previous studies of the electrochemical properties of electrodes fabricated using multilayered $Ti_3C_2T_x$[36] or V_2CT_x[16] assembled with alkali cations have shown outstanding pseudocapacitive performances (particularly in the acidic H_2SO_4 electrolyte) of these electrodes. In case of V_2CT_x, assembled multilayered flakes showed superior chemical and electrochemical stability compared to their single-layer flakes and dispersions. Therefore, we investigated the electrochemical properties of the freestanding MXene heterostructure films in three-electrode setups (similar to our previous work in [42]) using 3 M H_2SO_4 as the electrolyte. As shown in Fig. 4**a,** a cyclic voltammogram (CV) of a heterostructure Na-(50–50) film shows the electrochemical features observed in the CVs of multilayered $Ti_3C_2T_x$ and V_2CT_x with an overall improved electrochemical performance in terms of specific capacitance. In H_2SO_4 electrolytes, both $Ti_3C_2T_x$ and V_2CT_x, show distinct redox peaks located at around 0.3 V and 0 V (V vs Ag/AgCl), respectively. The heterostructure electrode shows the redox peaks corresponding to both MXenes. Interestingly, the heterostructure film, shows an almost constant capacitance (current response) in the tested potential window. With few exceptions, intercalation pseudocapacitive materials, including MXenes, have potential dependent capacitance and the maximum capacitance is delivered at a narrow potential range corresponding to the redox reactions. This is evident in CV profile of $Ti_3C_2T_x$, which delivers a large portion of its capacitance between −0.45 V and −0.2 V (vs. Ag/AgCl), highlighted in blue, and the Na-V_2CT_x which delivers most of

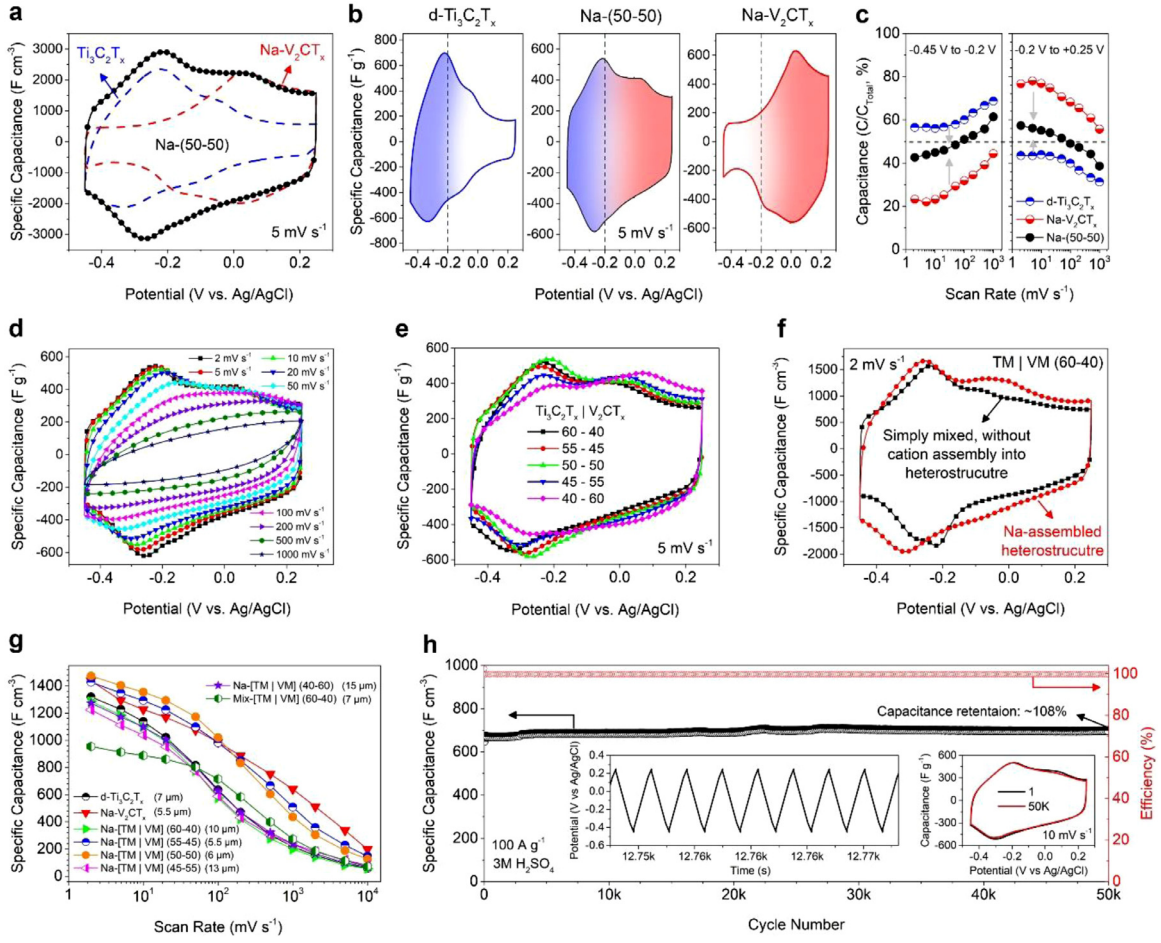

Fig. 4. Electrochemical characterization of MXene heterostructure electrodes in 3 M H_2SO_4. (a) Comparison between cyclic voltammograms (CVs) of $Ti_3C_2T_x$, Na-V_2CT_x, and Na-(50–50) MXene heterostructure at a scan rate of 5 mV s^{-1}. (b) Highlighted CVs of $Ti_3C_2T_x$, Na-V_2CT_x, and Na-(50–50) at the potential ranges in which these electrodes show their highest electrochemical activity. (c) Potential-limited capacitance to the total capacitance of $Ti_3C_2T_x$, Na-V_2CT_x, and Na-(50–50) at two potential ranges of (P-I), −0.45 V to −0.2 V and (P-II), −0.2 V to +0.25 V (V vs. Ag/AgCl) showing constant electrochemical response of the MXene heterostructure compared to $Ti_3C_2T_x$ MXene which delivers most of its capacitance only in P-I and Na-V_2CT_x, which is mostly active only in P-II. (d) CVs of Na-(50–50) at scan rates from 2 mV s^{-1} to 1000 mV s^{-1}. (e) CVs of MXene heterostructure film electrodes with different compositions at 5 mV s^{-1}. (f) Comparison between CVs of Na-assembled (60–40) MXene heterostructure and a film electrode prepared by simply mixing $Ti_3C_2T_x$ and V_2CT_x in 60:40 wt. ratio. (g) Volumetric capacitances of different electrodes tested in this study. The larger differences observed in capacitance values at higher rates might be due to the variations in electrode thicknesses. "TM" is $Ti_3C_2T_x$ MXene and "VM" is V_2CT_x MXene. (h) Cyclic performance of the Na-(50–50) electrode at a current density of 100 A g^{-1}.μ.

its capacitance from −0.2 V and +0.25 V (vs. Ag/AgCl), highlighted in red (shown in Fig. 4**b**). In the CV of the assembled heterostructure electrode, these two potential ranges have merged to deliver a constant current response (corresponding to a constant capacitance value) over the whole potential window (from −0.45 V to +025 V). To better demonstrate this property, a potential-limited capacitance (C, obtained from redox-dominant portions of CVs of individual MXenes) per total capacitance (C_{total}, obtained considering the whole potential window) for each of the three electrodes was calculated from CVs at various scan rates (shown in Fig. 4**c**) in the potential ranges of −0.45 V to −0.2 V (referred to as P-I) and −0.2 V to +0.25 V (referred to as P-II). Ideally it is preferred that pseudocapacitive electrodes deliver a capacitance independent of the potential range for a uniform power output at all voltages [43,44]. In the plot shown in Fig. 4c, such behavior can be translated to a 50% C/C_{Total} ratio, meaning that the electrode is delivering relatively similar capacitance (current output) at different points in its operating potential window. In the P-I range, the capacitance of Na-V_2CT_x is much smaller than the capacitance of $Ti_3C_2T_x$, while in P-II range Na-V_2CT_x delivers a higher capacitance. The Na-(50–50) MXene heterostructure electrode, however, shows a C/C_{Total} value of close to 50% in both potential ranges. Therefore, an important potential application of heterostructure MXene electrodes is designing better pseudocapacitive materials with uniform capacitance and possibly enlarged working potential window.

Fig. 4**d** shows CV profiles of a Na-(50–50) electrode at scan rates ranging from 2 mV s^{-1} to 1000 mV s^{-1} demonstrating the high-rate capability of the fabricated heterostructure electrodes. Fig. 4**e** shows the evolution of the CV profiles of heterostructure electrodes with various compositions. The intensity of redox peaks corresponding to V_2CT_x[16] and $Ti_3C_2T_x$[17] depends on the composition. The contributions from V_2CT_x redox couples increases with increasing its weight ratio in the heterostructure electrodes. We chose samples with a 50:50 ratio for our electrochemical studies as they showed the best overall electrochemical performance. Nevertheless, all other compositions showed the new CV features as well, with small variations (**Fig. S7** shows the CVs of different compositions at different scan rates). The pronounced presence of redox couples of both MXenes, however, was not present in the CV when $Ti_3C_2T_x$ and V_2CT_x MXenes were simply mixed without cation-mediated assembly. Fig. 4**f** compares the CVs of a simply mixed (without cations) and a Na assembled heterostructure film with a $Ti_3C_2T_x$:V_2CT_x weight ratio of 60:40. While the electrode prepared by simple colloidal mixing of the two MXenes still showed an improved pseudocapacitive behavior compared to the individual MXene electrodes, the redox peaks

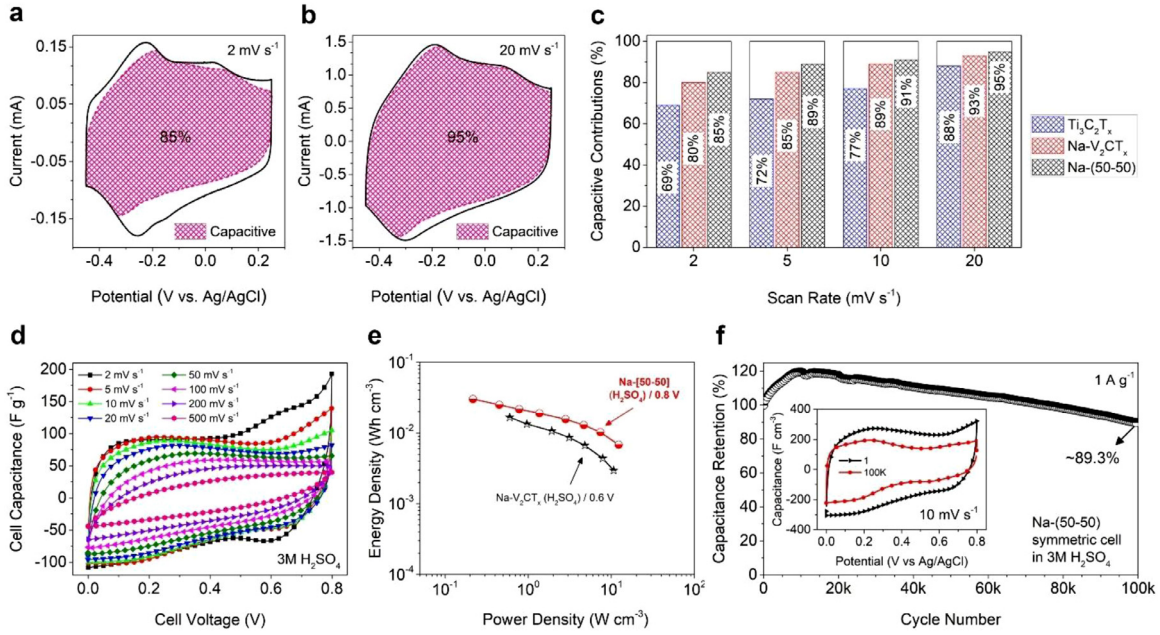

Fig. 5. Charge storage analyses and performance of the MXene heterostructure film electrodes in symmetric supercapacitors. Surface-controlled (capacitive) charge storage contributions to the overall charge stored at two scan rates of (a) 2 mV s^{-1} and (b) 20 mV s^{-1}. (c) Comparison between capacitive contributions in the overall charge storage performance of $Ti_3C_2T_x$, Na-V_2CT_x, and Na-(50–50) electrodes at scan rates of 2, 5, 10, and 20 mV s^{-1}, showing the improved capacitive response of the MXene heterostructure electrodes. (d) CVs of a symmetric supercapacitor cell with Na-(50–50) electrode in 3 M H_2SO_4 electrolyte. (e) Ragone plot comparing the power and energy densities of a symmetric cell fabricated using Na-(50–50) MXene heterostructure electrode to that of the previously reported state-of-the-art Na-V_2CT_x symmetric cell. (f) Cycle life of Na-(50–50) symmetric supercapacitor of heterostructure MXene electrodes at a current density of 1 A g^{-1} with capacitance retention of ~89.3% after 100,000 cycles.

related to V_2CT_x at more positive potentials was less pronounced compared to those in the heterolayered electrodes, probably because of the lower stability of pristine vanadium carbide MXene in the absence of cations [16]. Also, the ultra-large interlayer spacing of the mixed film (**Fig. S3**), possibly caused by the presence of remaining TBA^+ cations from the V_2CT_x solution, resulted in its poor volumetric capacitance. Fig. 4**g** compares the volumetric capacitance of the various heterostructure electrodes with pristine MXene electrodes. The highest volumetric capacitance of ~1473 F cm^{-3} and the gravimetric capacitance of ~ 410 F g^{-1} was achieved for Na-(50–50) heterostructure electrode (thickness of ~6 μm) at a scan rate of 2 mV s^{-1}. This electrode retained ~70% (~1020 F cm^{-3}) and ~30% (~436 F cm^{-3}) of its initial capacitance at scan rates of 100 mV s^{-1} and 1000 mV s^{-1}, respectively. Similar to other freestanding MXene film electrodes, the capacitance of the heterostructure electrodes showed a thickness-dependent behavior, however, because of the increased ion accessibility in these electrodes and the synergistic effects of two MXene layers, they could still deliver high capacitances at relatively high thicknesses. For example, a heterostructure film with a composition of Na-(40–60) and a thickness of ~15 μm could deliver a specific capacitance of ~1273 F cm^{-3} and ~402 F g^{-1} at a scan rate of 2 mV s^{-1}. These numbers are comparable to the capacitance of much thinner MXene electrodes, such as a 7 μm-thick pristine $Ti_3C_2T_x$ (~1319 F cm^{-3}, ~390 F g^{-1}) and a ~5.5 μm-thick Na-V_2CT_x (~1437 F cm^{-3}, ~423 F g^{-1}) at the same scan rate. In addition to their improved capacitances and rate-capability, the heterostructure MXene electrodes showed exceptional cycle life performances in highly acidic 3 M H_2SO_4 electrolyte. For example, a Na-(50–50) electrode showed no capacitance decay, and in fact, ‘8% capacitance increase (capacitance retention of ~108%) after 50,000 charge-discharge cycles at a current density of 100 A g^{-1} ($Ti_3C_2T_x$ and Na-V_2CT_x electrodes (**Fig. S8**) showed capacitance retentions of ~91% and 92%, respectively).

The contributions of the surface-controlled (capacitive) and diffusion-limited charge storage in a Na-(50–50) heterostructure electrode was evaluated and compared to those of $Ti_3C_2T_x$ and Na-V_2CT_x electrodes with similar thicknesses. Considering a power-law relationship between the current (i) and scan rate (v), $i = av^b$ (see the details in the Experimental Section) [45,46], a b-value of ~0.5 would indicate a mechanism controlled by diffusion while a b-value of ~1 is indicative of a surface-controlled charge storage mechanism [46]. As shown in Fig. 5**a, b** the capacitive contributions (hatched portions of the CVs) to the total charge stored in a Na-(50–50) heterostructure electrode at scan rates of 2 and 20 mV s^{-1} are ~86% and ~95%, respectively, which originate from fast surface-controlled reactions. These analyses show an improved capacitive response and ion transport properties for the heterostructure electrode compared to the pristine $Ti_3C_2T_x$ or V_2CT_x electrodes. For example, at a scan rate of 2 mV s^{-1} only ~69% and ~80% of the capacitances of $Ti_3C_2T_x$ and V_2CT_x come from fast surface reactions, respectively (charge analyses are shown in **Fig. S9–11**). Fig. 5**c** shows surface-controlled contributions for the three different electrodes at scan rates of 2, 5, 10, and 20 mV s^{-1}. It is evident that at all scan rates the heterostructure electrode shows a better capacitive performance. This improvement stems from the sequential assembly of $Ti_3C_2T_x$ and V_2CT_x in the heterolayered electrode architecture which hampers self-restacking of the individual MXene sheets and therefore, increases the accessible redox-active surface of the electrode [25,26,30], Electrochemical impedance spectroscopy results (**Fig. S12**) further confirmed the improved ion and charge transport properties of the heterostructure electrodes.

To investigate the real-device performance of the MXene heterostructure electrodes, symmetric supercapacitor cells were fabricated using Na-(50–50) electrodes and 3 M H_2SO_4 electrolyte. Fig. 5**d** shows the CV profiles of the symmetrical supercapacitor in a 0.8 V voltage window at scan rates from 2 to 500 mV s^{-1}. The calculated energy and power densities of a Na-(50–50) symmetric cell are shown in Fig. 5**e**, indicating an improved performance over symmetric cells made from Na-V_2CT_x in the same electrolyte [16]. The cells fabricated using heterostructure electrodes could deliver a power density of 0.03 W cm^{-3} at an energy density of ~0.22 Wh cm^{-3} and showed a maximum

energy density of ~12.3 Wh cm^{-3} at a power density of ~0.007 W cm^{-3}. Importantly, the symmetric supercapacitors of heterostructure MXene electrodes showed exceptional capacitance retention of ~89.3% after 100,000 charge-discharge cycles at a rate of 1 A g^{-1}. This outstanding cyclic performance renders MXene heterostructures as promising electrodes for practical energy storage devices that require consistent operation for a long time.

4. Conclusion

In summary, we have demonstrated self-assembly of two negatively charged MXene nanosheets: $Ti_3C_2T_x$ and V_2CT_x, into 2D heterostructures through a simple liquid phase assembly process capable of producing large amounts of material in a short time. The assembled MXenes showed a sequential stacking of few-layer $Ti_3C_2T_x$ and V_2CT_x in their structure confirmed by XRD and S/TEM analyses. Importantly, the change in the width and position of the XRD peaks corresponding to (0002) basal planes of the heterostructure MXene films showed that changing the $Ti_3C_2T_x$:V_2CT_x weight ratio plays a vital role in the stacking sequence and number of MXene layers in each stack of the assembly. The fabricated freestanding and binder-free MXene heterostructure films showed the characteristic redox peaks of both $Ti_3C_2T_x$ and V_2CT_x, which resulted in a more uniform capacitance in the entire tested potential window. The assembled heterostructure electrodes showed improved electrochemical behavior in 3 M H_2SO_4 electrolyte compared to their individual MXene building blocks with an exceptional cycle life performance with no capacity decay after 50,000 cycles, a high volumetric capacitance of ~1473 F cm^{-3}, and maximum volumetric power and energy densities of 0.03 W cm^{-3} and ~12.3 Wh cm^{-3}, respectively. This work demonstrates the promise of assembly of different MXene compositions into hetero-layered structures for the fabrication of high-performance energy storage devices.

Declaration of Competing Interest

The authors declare that they have no known competing financial interests or personal relationships that could have appeared to influence the work reported in this paper.

CRediT authorship contribution statement

Armin VahidMohammadi: Conceptualization, Formal analysis, Investigation, Methodology, Validation, Visualization, Writing - original draft. **Wentao Liang:** Formal analysis, Investigation, Methodology, Visualization. **Mehrnaz Mojtabavi:** Investigation, Methodology. **Meni Wanunu:** Funding acquisition, Methodology, Resources, Supervision, Writing - review & editing. **Majid Beidaghi:** Conceptualization, Funding acquisition, Project administration, Methodology, Resources, Supervision, Writing - review & editing.

Acknowledgments

Authors thank the Department of Materials Engineering at Auburn University for facilitating the access to XRD and SEM. TEM imaging was performed at Northeastern University's Kostas Advanced Nanocharacterization Facility (KANCF), Burlington, MA. This work was partially supported by Auburn University's Intramural Grants Program (IGP) and National Science Foundation grant (EFMA-1542707). M.B. acknowledges the support by a National Science Foundation grant (OAI-1929195). A.V.M. appreciates the support by Alabama EPSCoR Graduate Research Scholar Program (GRSP Round 12 and 13) doctoral fellowship.

Supplementary materials

Supplementary material associated with this article can be found, in the online version, at doi:10.1016/j.ensm.2021.06.014.

References

[1] E. Pomerantseva, Y. Gogotsi, Two-dimensional heterostructures for energy storage, Nat. Energy. 2 (2017) 17089, doi:10.1038/nenergy.2017.89.
[2] K.S. Novoselov, A. Mishchenko, A. Carvalho, A.H. Castro Neto, 2D materials and van der Waals heterostructures, Science (80-.) 353 (2016) aac9439–aac9439, doi:10.1126/science.aac9439.
[3] A.K. Geim, I.V. Grigorieva, Van der Waals heterostructures, Nature 499 (2013) 419–425, doi:10.1038/nature12385.
[4] D. Jariwala, T.J. Marks, M.C. Hersam, Mixed-dimensional van der Waals heterostructures, Nat. Mater. 16 (2017) 170–181, doi:10.1038/nmat4703.
[5] K. Kang, K.H. Lee, Y. Han, H. Gao, S. Xie, D.A. Muller, et al., Layer-by-layer assembly of two-dimensional materials into wafer-scale heterostructures, Nature 550 (2017) 229–233, doi:10.1038/nature23905.
[6] P. Xiong, X. Zhang, F. Zhang, D. Yi, J. Zhang, B. Sun, et al., Two-dimensional unilamellar cation-deficient metal oxide nanosheet superlattices for high-rate sodium ion energy storage, ACS Nano 12 (2018) 12337–12346, doi:10.1021/acsnano.8b06206.
[7] F. Shahzad, M. Alhabeb, C.B. Hatter, B. Anasori, S.M. Hong, C.M. Koo, et al., Electromagnetic interference shielding with 2D transition metal carbides (MXenes), Science 353 (2016) 1137–1140, doi:10.1126/science.aag2421.
[8] E. Lee, A. Vahidmohammadi, B.C. Prorok, Y.S. Yoon, M. Beidaghi, D.J. Kim, Room temperature gas sensing of two-dimensional titanium carbide (MXene), ACS Appl. Mater. Interfaces. 9 (2017) 37184–37190, doi:10.1021/acsami.7b11055.
[9] M. Mojtabavi, A. Vahidmohammadi, W. Liang, M. Beidaghi, M. Wanunu, Single-molecule sensing using nanopores in two-dimensional transition metal carbide (MXene) membranes, ACS Nano 13 (2019) 3042–3053, doi:10.1021/acsnano.8b08017.
[10] W. Bao, X. Tang, X. Guo, S. Choi, C. Wang, Y. Gogotsi, et al., Porous cryo-dried MXene for efficient capacitive deionization, Joule 2 (2018) 778–787, doi:10.1016/j.joule.2018.02.018.
[11] L. Ding, Y. Wei, L. Li, T. Zhang, H. Wang, J. Xue, et al., MXene molecular sieving membranes for highly efficient gas separation, Nat. Commun. 9 (2018) 155, doi:10.1038/s41467-017-02529-6.
[12] A. Vahidmohammadi, A. Hadjikhani, S. Shahbazmohamadi, M. Beidaghi, Two-dimensional vanadium carbide (MXene) as a high-capacity cathode material for rechargeable aluminum batteries, ACS Nano 11 (2017) 11135–11144, doi:10.1021/acsnano.7b05350.
[13] B. Anasori, M.R. Lukatskaya, Y. Gogotsi, 2D metal carbides and nitrides (MXenes) for energy storage, Nat. Rev. Mater. 2 (2017) 16098, doi:10.1038/natrevmats.2016.98.
[14] M. Naguib, V.N. Mochalin, M.W. Barsoum, Y. Gogotsi, 25th anniversary article: MXenes: a new family of two-dimensional materials, Adv. Mater. 26 (2014) 992–1005, doi:10.1002/adma.201304138.
[15] M.R. Lukatskaya, O. Mashtalir, C.E. Ren, Y. Dall'Agnese, P. Rozier, P.L. Taberna, et al., Cation intercalation and high volumetric capacitance of two-dimensional titanium carbide, Science 341 (2013) 1502–1505, doi:10.1126/science.1241488.
[16] A. VahidMohammadi, M. Mojtabavi, N.M. Caffrey, M. Wanunu, M. Beidaghi, Assembling 2D MXenes into highly stable pseudocapacitive electrodes with high power and energy densities, Adv. Mater. 31 (2019) 1806931, doi:10.1002/adma.201806931.
[17] M.R. Lukatskaya, S. Kota, Z. Lin, M.Q. Zhao, N. Shpigel, M.D. Levi, et al., Ultra-high-rate pseudocapacitive energy storage in two-dimensional transition metal carbides, Nat. Energy. 2 (2017) 17105, doi:10.1038/nenergy.2017.105.
[18] M. Naguib, O. Mashtalir, J. Carle, V. Presser, J. Lu, L. Hultman, et al., Two-dimensional transition metal carbides, ACS Nano 6 (2012) 1322–1331, doi:10.1021/nn204153h.
[19] N.C. Frey, J. Wang, G.I. Vega Bellido, B. Anasori, Y. Gogotsi, V.B. Shenoy, Prediction of synthesis of 2D metal carbides and nitrides (MXenes) and their precursors with positive and unlabeled machine learning, ACS Nano 13 (2019) 3031–3041, doi:10.1021/acsnano.8b08014.
[20] C. Chen, X. Xie, B. Anasori, A. Sarycheva, T. Makaryan, M. Zhao, et al., MoS_2-on-MXene heterostructures as highly reversible anode materials for lithium-ion batteries, Angew. Chemie - Int. Ed. 57 (2018) 1846–1850, doi:10.1002/anie.201710616.
[21] M.Q. Zhao, N. Trainor, C.E. Ren, M. Torelli, B. Anasori, Y. Gogotsi, Scalable manufacturing of large and flexible sheets of MXene/graphene heterostructures, Adv. Mater. Technol. 4 (2019) 1800639, doi:10.1002/admt.201800639.
[22] X. Dong, Y. Zhang, B. Ding, X. Hao, H. Dou, X. Zhang, Layer-by-layer self-assembled two-dimensional MXene/layered double hydroxide composites as cathode for alkaline hybrid batteries, J. Power Sources. 390 (2018) 208–214, doi:10.1016/j.jpowsour.2018.04.058.
[23] R. Zhao, M. Wang, D. Zhao, H. Li, C. Wang, L. Yin, Molecular-level heterostructures assembled from titanium carbide MXene and Ni-Co-Al layered double-hydroxide nanosheets for all-solid-state flexible asymmetric high-energy supercapacitors, ACS Energy Lett 3 (2018) 132–140, doi:10.1021/acsenergylett.7b01063.
[24] X. Wang, H. Li, H. Li, S. Lin, J. Bai, J. Dai, et al., Heterostructures of Ni-Co-Al layered double hydroxide assembled on V_4C_3 MXene for high-energy hybrid supercapacitors, J. Mater. Chem. A. 7 (2019) 2291–2300, doi:10.1039/c8ta11249e.
[25] J. Yan, C.E. Ren, K. Maleski, C.B. Hatter, B. Anasori, P. Urbankowski, et al., Flexible mxene/graphene films for ultrafast supercapacitors with outstanding volumetric capacitance, Adv. Funct. Mater. 27 (2017) 1701264, doi:10.1002/adfm.201701264.
[26] X. Jin, S.J. Shin, N. Kim, B. Kang, H. Piao, J.H. Choy, et al., Superior role of MXene nanosheet as hybridization matrix over graphene in enhancing interfacial electronic coupling and functionalities of metal oxide, Nano Energy 53 (2018) 841–848, doi:10.1016/j.nanoen.2018.09.055.
[27] C. Zhan, W. Sun, P.R.C. Kent, M. Naguib, Y. Gogotsi, D.E. Jiang, Computational screening of mxene electrodes for pseudocapacitive energy storage, J. Phys. Chem. C. 123 (2019) 315–321, doi:10.1021/acs.jpcc.8b11608.

[28] M. Ghidiu, M.R. Lukatskaya, M.Q. Zhao, Y. Gogotsi, M.W. Barsoum, Conductive two-dimensional titanium carbide “clay” with high volumetric capacitance, Nature 516 (2015) 78–81, doi:10.1038/nature13970.
[29] M. Naguib, R.R. Unocic, B.L. Armstrong, J. Nanda, Large-scale delamination of multi-layers transition metal carbides and carbonitrides “MXenes, Dalt. Trans. 44 (2015) 9353–9358, doi:10.1039/c5dt01247c.
[30] P. Xiong, R. Ma, N. Sakai, T. Sasaki, Genuine unilamellar metal oxide nanosheets confined in a superlattice-like structure for superior energy storage, ACS Nano 12 (2018) 1768–1777, doi:10.1021/acsnano.7b08522.
[31] P. Xiong, R. Ma, N. Sakai, L. Nurdiwijayanto, T. Sasaki, Unilamellar metallic MoS_2/graphene superlattice for efficient sodium storage and hydrogen evolution, ACS Energy Lett 3 (2018) 997–1005, doi:10.1021/acsenergylett.8b00110.
[32] P. Xiong, R. Ma, G. Wang, T. Sasaki, Progress and perspective on two-dimensional unilamellar metal oxide nanosheets and tailored nanostructures from them for electrochemical energy storage, Energy Storage Mater. (2018) 1–18, doi:10.1016/j.ensm.2018.12.011.
[33] X. Cai, T.C. Ozawa, A. Funatsu, R. Ma, Y. Ebina, T. Sasaki, Tuning the surface charge of 2d oxide nanosheets and the bulk-scale production of superlatticelike composites, J. Am. Chem. Soc. 137 (2015) 2844–2847, doi:10.1021/jacs.5b00317.
[34] H. Riazi, M. Anayee, K. Hantanasirisakul, A.A. Shamsabadi, B. Anasori, Y. Gogotsi, et al., Surface modification of a MXene by an aminosilane coupling agent, Adv. Mater. Interfaces. 1902008 (2020) 1–8, doi:10.1002/admi.201902008.
[35] W. Tian, A. VahidMohammadi, Z. Wang, L. Ouyang, M. Beidaghi, M.M. Hamedi, Layer-by-layer self-assembly of pillared two-dimensional multilayers, Nat. Commun. 10 (2019) 2558, doi:10.1038/s41467-019-10631-0.
[36] D. Zhao, M. Clites, G. Ying, S. Kota, J. Wang, V. Natu, et al., Alkali-induced crumpling of Ti_3C_2Tx (MXene) to form 3D porous networks for sodium ion storage, Chem. Commun. 54 (2018) 4533–4536, doi:10.1039/c8cc00649k.
[37] V. Natu, M. Clites, E. Pomerantseva, M.W. Barsoum, Mesoporous MXene powders synthesized by acid induced crumpling and their use as Na-ion battery anodes, Mater. Res. Lett. 6 (2018) 230–235, doi:10.1080/21663831.2018.1434249.
[38] M. Ghidiu, S. Kota, J. Halim, A.W. Sherwood, N. Nedfors, J. Rosen, et al., Alkylammonium Cation Intercalation into Ti_3C_2 (MXene): effects on Properties and Ion-Exchange Capacity Estimation, Chem. Mater. 29 (2017) 1099–1106, doi:10.1021/acs.chemmater.6b04234.
[39] M. Onoda, Z. Liu, Y. Ebina, K. Takada, T. Sasaki, X-ray diffraction study on restacked flocculates from binary colloidal nanosheet systems $Ti_{0.91}O_2$-MnO_2, $Ca_2Nb_3O_{10}$-$Ti_{0.91}O_2$, and $Ca_2Nb_3O_{10}$-MnO_2, J. Phys. Chem. C. 115 (2011) 8555–8566, doi:10.1021/jp201477w.
[40] X. Jin, S.J. Shin, N. Kim, B. Kang, H. Piao, J.H. Choy, et al., Superior role of MXene nanosheet as hybridization matrix over graphene in enhancing interfacial electronic coupling and functionalities of metal oxide, Nano Energy 53 (2018) 841–848, doi:10.1016/j.nanoen.2018.09.055.
[41] A. Lipatov, H. Lu, M. Alhabeb, B. Anasori, A. Gruverman, Y. Gogotsi, et al., Elastic properties of 2D Ti_3C_2Tx MXene monolayers and bilayers, Sci. Adv. 4 (2018) eaat0491, doi:10.1126/sciadv.aat0491.
[42] W. Tian, A. VahidMohammadi, M.S. Reid, Z. Wang, L. Ouyang, J. Erlandsson, et al., Multifunctional nanocomposites with high strength and capacitance using 2D MXene and 1D nanocellulose, Adv. Mater. (2019) 1902977 1902977, doi:10.1002/adma.201902977.
[43] P. Simon, Y. Gogotsi, Materials for electrochemical capacitors, Nat. Mater. 7 (2008) 845–854, doi:10.1038/nmat2297.
[44] Y. Gogotsi, R.M. Penner, Energy storage in nanomaterials – capacitive, pseudocapacitive, or battery-like? ACS Nano 12 (2018) 2081–2083, doi:10.1021/acsnano.8b01914.
[45] V. Augustyn, J. Come, M.A. Lowe, J.W. Kim, P.L. Taberna, S.H. Tolbert, et al., High-rate electrochemical energy storage through Li + intercalation pseudocapacitance, Nat. Mater. 12 (2013) 518–522, doi:10.1038/nmat3601.
[46] J. Wang, J. Polleux, J. Lim, B. Dunn, Pseudocapacitive contributions to electrochemical energy storage in TiO_2 (Anatase) nanoparticles, J. Phys. Chem. C. 111 (2007) 14925–14931, doi:10.1021/jp074464w.
[47] A. Lipatov, M. Alhabeb, M.R. Lukatskaya, A. Boson, Y. Gogotsi, A. Sinitskii, Effect of synthesis on quality, electronic properties and environmental stability of individual monolayer Ti_3C_2 MXene flakes, Adv. Electron. Mater. 2 (2016) 1600255, doi:10.1002/aelm.201600255.
[48] M. Naguib, J. Halim, J. Lu, K.M. Cook, L. Hultman, Y. Gogotsi, et al., New two-dimensional niobium and vanadium carbides as promising materials for Li-ion batteries, J. Am. Chem. Soc. 135 (2013) 15966–15969, doi:10.1021/ja405735d.
[49] A. Vahidmohammadi, J. Moncada, H. Chen, E. Kayali, J. Orangi, C.A. Carrero, et al., Thick and freestanding MXene/PANI pseudocapacitive electrodes with ultrahigh specific capacitance, J. Mater. Chem. A. 6 (2018) 22123–22133, doi:10.1039/c8ta05807e.
[50] M. Alhabeb, K. Maleski, B. Anasori, P. Lelyukh, L. Clark, S. Sin, et al., Guidelines for synthesis and processing of two-dimensional titanium carbide (Ti_3C_2Tx MXene), Chem. Mater. 29 (2017) 7633–7644, doi:10.1021/acs.chemmater.7b02847.